Space and Time Shape Constrained Deformable Surfaces for 4D Medical Image Segmentation

Johan Montagnat, Hervé Delingette

Space and Time Shape Constrained Deformable Surfaces for 4D Medical Image Segmentation

Montagnat J. and Delingette H.
INRIA Sophia, BP 93, 06902 Sophia-Antipolis Cedex France
http://www-sop.inria.fr/epidaure/

Abstract

The heart motion study is vital for the understanding and the early diagnosis of cardiac pathologies that remain the primary cause of death in western countries to date. Heart motion analysis require the extraction of quantitative parameters from time sequences of 3D images (4D images) such as volume, septum wall thickness, ejection fraction and motion amplitude. In this paper, we propose a framework for the reconstruction of the left ventricle motion from 4D images based on 4D deformable surface models. These 4D models are represented as a time sequence of 3D meshes whose deformation are correlated during the cardiac cycle. Both temporal and spatial constraints are combined to introduce a prior knowledge of the heart motion and improve the segmentation accuracy. When compared to previous approaches, our framework appears too be more efficient and more powerful since it can also include the notion of trajectory constraint. We have validated this segmentation tool and its ability to segment even noisy or low contrasted images on 4D MR, SPECT and ultrasound images.

1 Context

Recently, the improvement of medical image acquisition technology has allowed the production of time sequences of 3D medical images (3D+T or 4D images) for several image modalities (CT, MRI, US, SPECT...). Tagged MRI is the gold standard of heart motion analysis since it is the only modality permitting the extraction of the motion of physical points located in the myocardium [18]. However, other modalities may be used for meaningful parameters extraction at a lower cost. In particular, the fast development of 3D ultrasound imaging is very promising for performing cardiac motion analysis due to its accessibility and low cost [17].

The main target for these new ultra-fast image acquisition devices is to capture and analyze the heart motion through the extraction of quantitative parameters such as volume, septum wall thickness, ejection fraction and motion amplitude. However, in order to estimate these parameters, it is necessary to reconstruct the left ventricle motion during a cardiac cycle. Tracking the ventricle motion in 2D or 3D image sequences has been the motivation for much research work [10, 9, 2]. Tracking [12, 16] and motion analysis [4, 7] based on deformable models in 4D images take into account the time continuity and periodicity to improve their robustness.

models. Our concept of 4D deformable surface models combines spatial and time constraints which differs from most previous approaches [12, 16, 4] that decouple them. Furthermore, unlike the strategy presented in [7], the motion estimation is not parameterized by a global time-space transformation. It leads to more efficient computation and more possible variability in the motion that is being recovered. Finally, our approach can include the notion of trajectory shape constraint which is the generalization of the shape memory constraint. The adaptability of the segmentation tool is demonstrated through various imaging modalities segmentation.

2 4D Deformable Models

Let us denote I a 4D image composed of n volumetric images corresponding to n different instants $\{t_0, \ldots, t_{n-1}\}$. We define a 4D deformable model $\mathcal{S}$ as a set of n deformable surfaces $\{\mathcal{S}_t\}_{t\in[0,n-1]}$, each surface model $\mathcal{S}_t$ representing a given anatomical structure at instant t. Among the possible geometric representations of deformable surfaces (see [13] for a survey on deformable models), we have chosen to use the *simplex meshes* [8] discrete surface representations. They are defined by a set of vertices and a constant connectivity function. Their main advantage lies in their simple data structure permitting an efficient implementation both in terms of computational time and memory storage. This is specifically important in the case of 4D deformable models where n surface meshes must be updated at each iteration. Furthermore, simplex meshes are especially well-suited for the computation of curvature-based regularizing forces. In order to keep an efficient implementation, all n surface meshes $\mathcal{S}_t$ have the same topology, *i.e.* there is a one to one correspondence between the d vertices composing each surface. In the rest of the paper, $\mathbf{p}_{i,t}$ denotes the position of vertex number i at time t.

A 4D model deforms under the combined action of three forces aiming at recovering the motion of an anatomical structure: (i) the data, or *external*, force attracts each vertex towards the structure boundaries; (ii) the spatial regularizing, or *internal*, force ensures the smoothness of the deforming surface by introducing spatial continuity constraints in the deformation process; (iii) the temporal regularizing force similarly relies on a prior knowledge on the time dimension continuity to regularize the deformation process. A second order (Newtonian) evolution scheme discretized using an explicit scheme governs the deformation of each vertex (see [8] for details):

$$\mathbf{p}_{i,t}^{k+\Delta k} = \mathbf{p}_{i,t}^{k} + (1-\gamma)(\mathbf{p}_{i,t}^{k} - \mathbf{p}_{i,t}^{k-\Delta k}) + \alpha_i f_{\text{int}}(\mathbf{p}_{i,t}^{k}) + \delta_i f_{\text{time}}(\mathbf{p}_{i,t}^{k}) + \beta_i f_{\text{ext}}(\mathbf{p}_{i,t}^{k}), \quad (1)$$

where f_{int}, f_{time}, and f_{ext} are the internal, the temporal, and external forces respectively. α_i, β_i, and δ_i are weights including the vertex mass and the iteration step Δk. In all our experiments, the background damping γ is fixed to value 0.35 based on an empirical study showing that this value optimizes the convergence speed in general.

Simplex meshes provide a powerful framework for computing internal regularizing forces [8] including smoothing forces without shrinking side effect. External forces are computed as distance functions of the model vertices to the data. This speeds-up the model convergence compared to potential fields approaches and it avoids oscillations [5]. Deformations are computed along each vertex normal direction to avoid

discriminate boundary voxel in images. By lack of space, the computation of external forces are not discussed here and the reader may refer to [15] for details.

3 Shape and Temporal Constraints

The main incentive for performing medical image segmentation based on deformable models lies in their ability to incorporate a prior knowledge on the data that is being recovered. In most cases, this knowledge is translated mathematically into a set of regularizing constraints that greatly improves the robustness and accuracy of the segmentation process against noise and outliers. Indeed, many methods have been proposed in the literature to regularize deformations including parameterized [20] or modal [6] representations with a limited number of parameters, and the control of the deformation process through global transformations [3] or free-form deformations [11].

We introduce two complementary constraints that are specifically suited for the left ventricle tracking in 4D images. The former consists of a shape constraint that tends to enforce 3D geometric continuity. The latter is a temporal constraint that causes a 4D mesh to rely on a prior motion knowledge. It is important to note that, unlike many previous work, in our framework both constraints are applied simultaneously thus leading to a true 4D approach. Furthermore, each constraint can encapsulate a weak or strong prior knowledge, as summarized in table 1.

Prior knowledge	Spatial constraint	Temporal constraint
Weak	Curvature-based shape smoothing	Temporal position averaging
Strong	Shape memory constraint	Trajectory memory constraint

Table 1: Description of the different spatial and temporal constraint depending of the amount of a priori knowledge.

3.1 Shape Constraints

In the case where no reference shape is known (weak shape constraint), we use the regularizing force defined in [8], that minimizes the variation of mean-curvature over the mesh. Otherwise, we add an additional shape constraint force f_{shape} that is related to a reference shape $\mathcal{S}'$ of the anatomical structure. This constraint extends the globally-constrained deformation scheme described in [14] to the 4D case and introduce shape prior knowledge. Let $\mathcal{S}^k$ denotes the 4D model after the k^{th} iteration. At each iteration, external forces f_{ext} are computed for each vertex so that $\mathbf{p}_{i,t} + f_{\text{ext}}(\mathbf{p}_{i,t})$ corresponds to the myocardium boundary point that best matches $\mathbf{p}_{i,t}$. We estimate a global transformation T^k belonging to a given group of transformations (*e.g.* the affine transformation group $\mathrm{T}_{\text{affine}}$) that approximates the external force field by minimizing the least square criterion:

$$T^k = \arg \min_{T \in \mathrm{T}_{\text{affine}}} \left\{ \sum_{t=0}^{n-1} \sum_{i=0}^{d-1} \left\| T(\mathbf{p}_{i,t}) - (\mathbf{p}_{i,t} + f_{\text{ext}}(\mathbf{p}_{i,t})) \right\|^2 \right\}. \quad (2)$$

remains identical to $\mathcal{S}'^0$ up to an affine transformation. A shape force is defined on each vertex of $\mathcal{S}^k$ as a spring-like force towards its updated reference position: $f_{\text{shape}}(\mathbf{p}_{i,t}^k) = \mathbf{p}_{i,t}^k \mathbf{p}_{i,t}'^k$.

Furthermore, a *locality* parameter λ is introduced to weight the influence of the shape force relative to the internal and external forces as described in [14]:

$$\begin{aligned}\mathbf{p}_{i,t}^{k+\Delta k} &= \mathbf{p}_{i,t}^k + (1-\gamma)(\mathbf{p}_{i,t}^k - \mathbf{p}_{i,t}^{k-\Delta k}) + \\ &\quad \lambda(\alpha_i f_{\text{int}}(\mathbf{p}_{i,t}^k) + \delta_i f_{\text{time}}(\mathbf{p}_{i,t}^k) + \beta_i f_{\text{ext}}(\mathbf{p}_{i,t}^k)) + (1-\lambda) f_{\text{shape}}(\mathbf{p}_{i,t}^k).\end{aligned}$$

When $\lambda = 0$, the 4D model is deformed through the application of a global affine transformation from its reference shape. Conversely, if $\lambda = 1$, only the weak shape constraint applies. Any intermediate value of λ produces local deformations combined with a shape constraint.

3.2 Temporal Constraints

The temporal regularizing force f_{time} is also defined as a spring-like force $f_{\text{time}}(\mathbf{p}_{i,t}) = \tilde{\mathbf{p}}_{i,t} - \mathbf{p}_{i,t}$ attracting vertex $\mathbf{p}_{i,t}$ towards a point $\tilde{\mathbf{p}}_{i,t}$. When no prior knowledge is used. we define a week temporal constraint by attracting $\mathbf{p}_{i,t}$ towards the middle position of its two temporal neighbors :$\tilde{\mathbf{p}}_{i,t} = \frac{\mathbf{p}_{i,t-1} + \mathbf{p}_{i,t+1}}{2}$. Applying this force is equivalent to minimizing the speed of each vertex, and therefore minimizing the kinetic energy of the 4D model.

When using *a priori* information regarding the trajectory of each vertex, we determine $\tilde{\mathbf{p}}_{i,t}$ such that this point lies on the ideal vertex trajectory. It is important to note that these trajectories may not correspond to trajectories of physical points lying on the myocardium but are only used as temporal constraints. To store each *a priori* vertex trajectory, we could store the n vertex positions $\{\mathbf{p}_{i,t}\}_{t\in[0,n-1]}$ of the same vertex over time. However, this representation would require that the current vertex $\mathbf{p}_{i,t}$ has the same orientation and scale than its reference trajectory, which is not usually the case. Instead, we choose to store the trajectory, which is a closed 3D curve (due to the periodicity of the cardiac motion), as a set of geometric parameters $\{\varepsilon_{i,t}, \varphi_{i,t}, \psi_{i,t}\}$ that are invariant to rotation, translation and scale. Intuitively, $\varepsilon_{i,t}$, $\varphi_{i,t}$, and $\psi_{i,t}$ correspond to discrete arc length, curvature, and torsion respectively.

We now describe in more details the definition of the three parameters $\{\varepsilon_{i,t}, \varphi_{i,t}, \psi_{i,t}\}$. First, each vertex $\mathbf{p}_{i,t}$ has two temporal neighbors $\mathbf{p}_{i,t-1}$ and $\mathbf{p}_{i,t+1}$. Let $\mathbf{p}_{i,t}^{\perp}$ denotes the orthogonal projection of $\mathbf{p}_{i,t}$ onto $[\mathbf{p}_{i,t-1}, \mathbf{p}_{i,t+1}]$. The relative position of point $\mathbf{p}_{i,t}$ to its temporal neighbors may be defined through: (i) the *metric parameter* $\varepsilon_{i,t}$ measuring the relative position of $\mathbf{p}_{i,t}^{\perp}$ in segment $[\mathbf{p}_{i,t-1}, \mathbf{p}_{i,t+1}]$; (ii) the angle $\varphi_{i,t}$ measuring the elevation of $\mathbf{p}_{i,t}$ above the segment $[\mathbf{p}_{i,t-1}, \mathbf{p}_{i,t+1}]$ in plane $(\mathbf{p}_{i,t-1}, \mathbf{p}_{i,t}, \mathbf{p}_{i,t+1})$; and (iii) the angle $\psi_{i,t}$ measuring the discrete torsion of the trajectory. Let $\mathbf{t}_{i,t}$ denote the discrete tangent, $\mathbf{b}_{i,t}$ the binormal vector, and $\mathbf{n}_{i,t}$ the discrete normal to point $\mathbf{p}_{i,t}$ respectively:

$$\mathbf{t}_{i,t} = \frac{\mathbf{p}_{i,t-1}\mathbf{p}_{i,t+1}}{||\mathbf{p}_{i,t-1}\mathbf{p}_{i,t+1}||},\ \mathbf{b}_{i,t} = \frac{\mathbf{p}_{i,t}\mathbf{p}_{i,t+1} \wedge \mathbf{p}_{i,t-1}\mathbf{p}_{i,t}}{||\mathbf{p}_{i,t}\mathbf{p}_{i,t+1} \wedge \mathbf{p}_{i,t-1}\mathbf{p}_{i,t}||},\ \mathbf{n}_{i,t} = \mathbf{b}_{i,t} \wedge \mathbf{t}_{i,t}.$$

The metric parameter is defined by $\varepsilon_{i,t} = \frac{||\mathbf{p}_{i,t}^{\perp}\mathbf{p}_{i,t+1}||}{||\mathbf{p}_{i,t-1}\mathbf{p}_{i,t+1}||}$, the elevation angle is $\varphi_{i,t} =$

$$\mathbf{r}_{i,t} = \frac{\mathbf{t}_{i,t} \wedge (\mathbf{p}_{i,t-2}\mathbf{p}_{i,t-1} \wedge \mathbf{p}_{i,t+1}\mathbf{p}_{i,t+2})}{\|\mathbf{t}_{i,t} \wedge (\mathbf{p}_{i,t-2}\mathbf{p}_{i,t-1} \wedge \mathbf{p}_{i,t+1}\mathbf{p}_{i,t+2})\|} \text{ and } \mathbf{n}_i = \cos(\psi_{i,t})\mathbf{r}_{i,t} + \sin(\psi_{i,t})\mathbf{t}_{i,t} \wedge \mathbf{r}_{i,t}.$$

Figure 1 illustrates the elements composing the trajectory geometry.

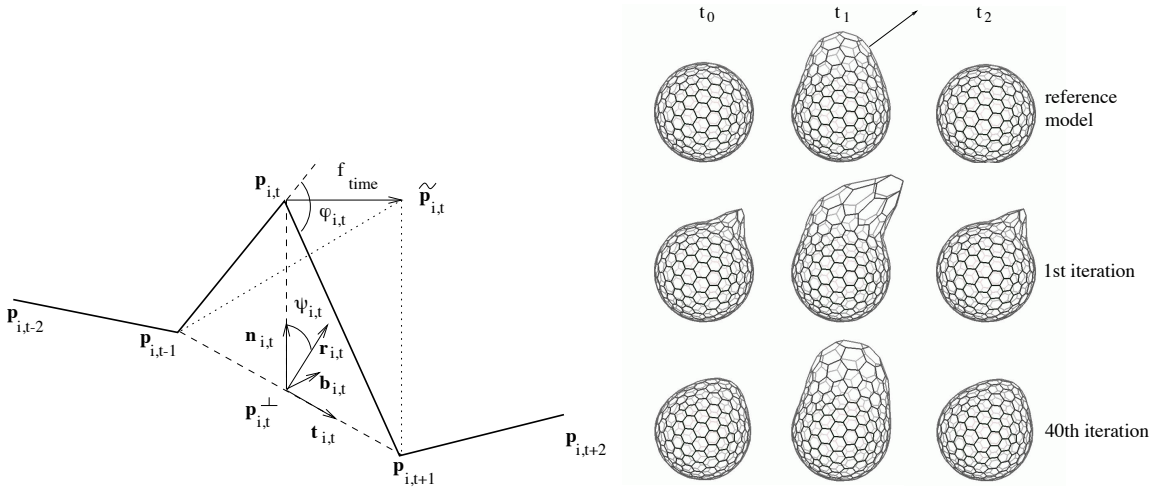

Figure 1: Left: Trajectory geometry and temporal force. Right: temporal force effect.

The position of $\mathbf{p}_{i,t}$ is related to the position of its neighbors and the trajectory parameters by equation:

$$\mathbf{p}_{i,t} = \varepsilon_{i,t}\mathbf{p}_{i,t-1} + (1-\varepsilon_i)\mathbf{p}_{i,t+1} + h(\varepsilon_{i,t}, \varphi_{i,t}, \mathbf{p}_{i,t-1}, \mathbf{p}_{i,t+1})(\cos(\psi_{i,t})\mathbf{r}_{i,t} + \sin(\psi_{i,t})\mathbf{t}_{i,t} \wedge \mathbf{r}_{i,t}), \quad (3)$$

where $h = \|\mathbf{p}_{i,t}\mathbf{p}^{\perp}_{i,t}\|$. The temporal force is computed with $\tilde{\mathbf{p}}_{i,t}$ defined by equation 3 using the trajectory reference parameters.

Figure 1 shows the temporal constraint effect. A spherical 4D model composed of 3 instants (t_0, t_1, and t_2) is shown in the upper row. A single vertex of the model is submitted to an external force at time t_1. The middle row shows the resulting deformation. Surface $\mathcal{S}_1$ is deformed causing surfaces $\mathcal{S}_0$ and $\mathcal{S}_2$ to deform through the temporal constraint, although the deformation is attenuated in time. The bottom row shows the surface converging towards its reference motion after 40 iterations.

3.3 Initialization procedure

In general, to get a first rough position of the 4D left ventricle model, we first proceed by using only highly constrained spatial deformations without any temporal constraint. By using $\lambda = 0$, we basically estimate a set of global affine transformations to align the model with the 4D dataset. Then, we proceed by iteratively increasing the locality parameter λ while adding temporal constraints. This approach allows an evolutional deformation scheme based on a coarse-to-fine strategy.

4.1 MR Images

Cardiac MR images have a very accurate resolution in slice planes (here 256×256 voxels). However, the third dimension resolution is much lower (the anisotropic ratio is about 8). We show a segmentation experiment on a sequence composed of 13 images each having 9 slices covering the heart left ventricle. The cardiac MR images contrast varies between slices and the heart boundaries are poorly defined.

A 4D model is generated by embedding a set of identical ellipsoids roughly centered on the left ventricle in the first image sequence. Only spatial and temporal smoothing (weak) constraints are used since no relevant prior information was given. The local deformations are constrained by a global affine transformation. A low locality coefficient ($\lambda < 40\%$) prevents the surface from being too sensitive to the lack of information in area where the gradient filter gave no response. The α, β and δ weights are constant ($\alpha = 1$, $\beta = 0.15$, $\delta = 0.1$). Each surface model is composed of 500 vertices and the deformation process for the whole 4D model only takes 1 min 46 s on a 500 MHz Digital PWS with 512 Mb of memory. Four out of the 13 surfaces composing the 4D model are shown in figure 2 on the left. The middle graph plots the volume variation curve. It corresponds to a non pathological volume curve.

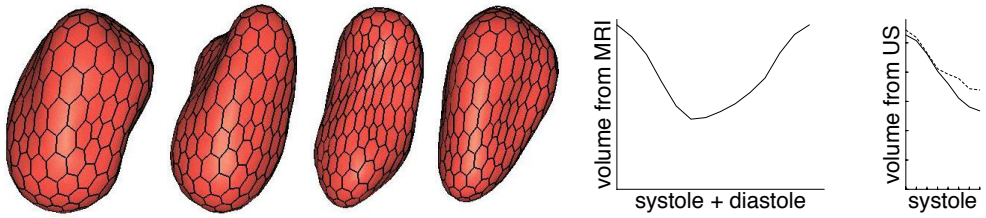

Figure 2: Left: 4 surfaces from the 4D models deformed in an MRI. Middle: 4D model volume curve. Right: 4D model volume obtained from a US image by 3D (dashed line) and 4D (solid line) segmentation.

4.2 SPECT Images

We have processed a 4D SPECT image database including healthy and pathological patients. Each sequence is composed of eight 3D images covering a complete cardiac cycle. The systole is approximatively three instants long whereas the diastole takes the remaining five instants. Each 3D image is composed of 64^3 voxels acquired on a regular grid. We compare images of healthy patients with a normal endocardium blood perfusion and pathological patients with an abnormal perfusion due to some ischemic zones. The mean deformation time for all 4D models, made of 700 vertex surfaces, is 2 min 34 s.

The reference model is built from an healthy patient image by 3D segmentation. The high image contrast allows to use gradient information to compute external forces. The 3D segmentation does not involve any time continuity constraints. A 4D deformation stage with time smoothing forces is therefore needed to obtain a reference

the segmentation of low contrasted images showing pathologies such as ischemia. Due to the similarity between images, the 4D model is roughly initialized in its reference position. Rigid then similarity registration are first used to compensate the differences in location and size between patients. Local deformations with an affine constraint are then used. By progressively increasing the locality factor and lowering the external forces range, local deformations only affect a restricted neighborhood.

Figure 3 shows a frontal view of the 4D models. Top line displays the reference model obtained by 3D segmentation and revealing poor time continuity. The center line displays the 4D model regularized by time smoothing constraints in the image of a healthy patient. The bottom line shows the model extracted from a pathological case. The surface model reveals the pathological heart with weak motion amplitude.

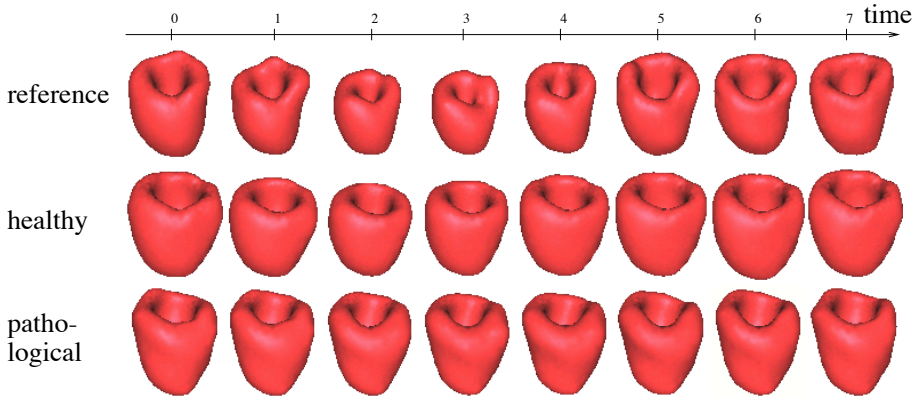

Figure 3: 4D models of the myocardium: reference model obtained by 3D segmentation (top row), healthy case (middle row), and pathological case (bottom row).

4.3 Ultrasound Images

The speckle noise of ultrasound images and the lack of beam reflection on boundaries tangent to the ultrasound rays make the segmentation process difficult. 4D ultrasound images are composed by a set of slices acquired with a rotative probe [15] with a low spatial (20 degrees of arc) and time (8 instants) resolution. A 4D model is built as in the isotropic example, by 3D segmentation of a reference image. The model is first registered by a similarity to align and adapt its scale to the data. The gradient information is sufficient since the deformations are strongly constrained to speed-up the model convergence. A large force range allows the model to find boundaries far from the initial model position. After registration, the model locally deforms with an affine global constraint. Local deformations guided by region based forces with a restricted range are used in the final segmentation. The use of region-based forces slows down the deformation process. The deformation time for the 4D model was 4 min 42 s.

Figure 2, right, shows the time evolution of the heart left ventricle (solid line). The volume is compared to the result of an iterative 3D segmentation of the same sequence from an earlier study [15] (dashed line). The time regularizing constraints make the 4D curve much more regular. The initial volume value is very close (3%

tends to accumulate errors. Moreover, the 4D curves shows a profile closer from the theoretical line expected. The model volume leads to a 49% ejection fraction. This value compares to the 45% ejection fraction computed from a manual segmentation by a cardiologist on the same sequence.

Figure 4 shows the sequence slices on which are superimposed the model intersections with each plane. The 8 figure columns correspond to the 8 instants. Five rows corresponding to one slice out of two (from top to bottom: 0, 40, 80, 120, and 160 degrees of arc) are shown.

5 Conclusion

We have demonstrated the ability of 4D models to track the left ventricle motion in 4D noisy medical images. The proposed framework relies on complementary spatial and temporal constraints to regularize the deformation while introducing a priori knowledge about the ventricle shape and motion in the segmentation process. Shape constraints allow the segmentation of sparse and low contrast data. This approach leads to an endocardium surface modeling well suited for estimating quantitative parameters such as endocardium volume or wall thickness.

Acknowledgements

We are grateful to GE medical system, Prof. Goris of the University of Stanford Medical School and Dr Lethor of CHU Barbois for MRI, SPECT and US image acquisitions respectively. Special thanks go to Tal Arbel for proof-reading.

References

[1] E. Bardinet, L. Cohen, and N. Ayache. Tracking and motion analysis of the left ventricle with deformable superquadrics. *Medical Image Analysis*, 1(2):129–149, 1996.

[2] M.-O. Berger, G. Winterfeldt, and J.-P. Lethor. Contour Tracking in Echocardiographic Sequences without Learning Stage: Application to the 3D Reconstruction of the 3D Beating Left Ventricle. In *MICCAI*, vol. 1679 of LNCS, 508–515, 1999.

[3] P. Besl and N. McKay. A method for registration of 3D shapes. *IEEE Transaction on Pattern Analysis and Machine Intelligence*, 14(2):239–256, February 1992.

[4] P. Clarysse, D. Friboulet, and I. Magnin. Tracking Geometrical Descriptors on 3-D Deformable Surfaces: Application to the Left-Ventricular Surface of the Heart. *IEEE Transaction on Medical Imaging*, 16(4):392–404, 1997.

[5] L.D. Cohen. On Active Contour Models and Balloons. *Computer Vision, Graphics, and Image Processing: Image Understanding*, 53(2):211–218, 1991.

[6] T.F. Cootes, C.J. Taylor, D.H. Cooper, and J. Graham. Active shape models, their training and application. *Computer Vision and Image Understanding*, 61(1):38–59, 1995.

[7] J. Declerck, J. Feldmar, and N. Ayache. Definition of a 4D continuous planispheric transformation for the tracking and the analysis of LV motion. *Medical Image Analysis*, 2(2):197–213, 1998.

[8] H. Delingette. General Object Reconstruction based on Simplex Meshes. *International Journal of Computer Vision*, 32(2):111–146, 1999.

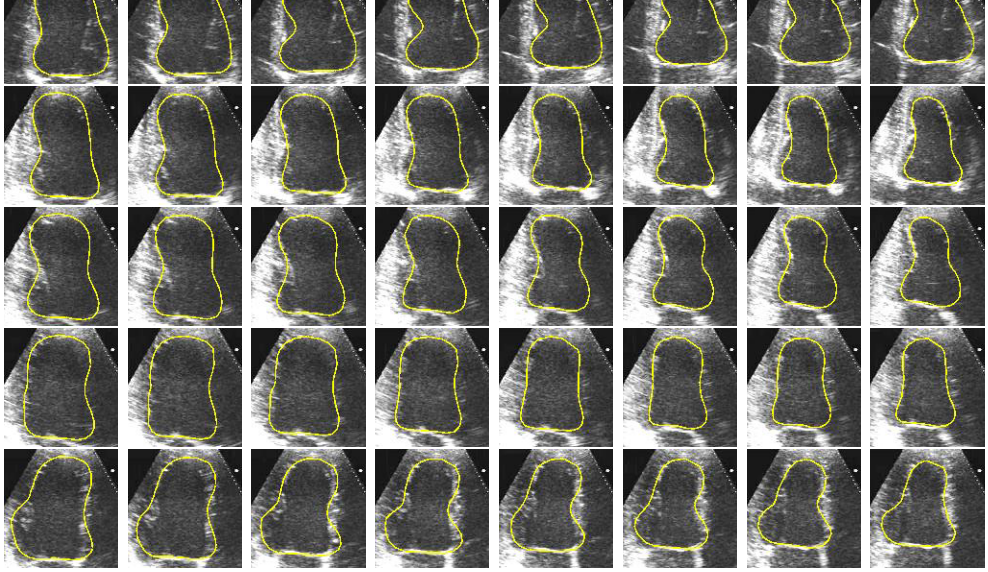

Figure 4: Set of slices of the ultrasound image superimposed with the deformed model intersection. From left to right: cardiac sequence instant. From top to bottom: slices oriented with angle 0, 40, 80, 120, and 160 degrees of arc.

[9] A. Giachetti. On-line analysis of echocardiographic image sequences. *Medical Image Analysis*, 2(3):261–284, 1998.

[10] G. Jacob, A. Noble, M. Mulet-Parada, and A. Blake. Evaluating a robust contour tracker on echocardiographic sequences. *Medical Image Analysis*, 3(1):63–75, 1999.

[11] J. Lötjönen, P.-J. Reissman, I. Magnin, and T. Katila. Model extraction from magnetic resonance volume data using the deformable pyramid. *Medical Image Analysis*, 3(4):387–406, 1999.

[12] J. McEachen and J. Duncan. Shaped-base tracking of left ventricular wall motion. *IEEE Transaction on Medical Imaging*, 16(3):270–283, 1997.

[13] T. McInerney and D. Terzopoulos. Deformable models in medical image analysis: a survey. *Medical Image Analysis*, 1(2):91–108, 1996.

[14] J. Montagnat and H. Delingette. Globally constrained deformable models for 3D object reconstruction. *Signal Processing*, 71(2):173–186, 1998.

[15] J. Montagnat, H. Delingette, and G. Malandain. Cylindrical Echocardiographic Images Segmentation based on 3D Deformable Models. In *MICCAI*, vol. 1679 of LNCS, 168–175, 1999.

[16] C. Nastar and N. Ayache. Frequency-Based Nonrigid Motion Analysis: Application to Four Dimensional Medical Images. *IEEE Transaction on Pattern Analysis and Machine Intelligence*, 18(11):1067–1079, 1996.

[17] X. Papdemetris, A. Sinusas, D. Dione, and J. Duncan. 3D Cardiac Deformation from Ultrasound Images. In *MICCAI*, vol. 1679 of LNCS, 420–429, 1999.

[18] J. Park, D. Metaxas, and L. Axel. Analysis of LV motion based on volumetric deformable models and MRI-SPAMM. *Medical Image Analysis*, 1(1):53–71, 1996.

[19] D. Terzopoulos, A. Witkin, and M. Kass. Constraints on Deformable Models: Recovering 3D Shape and Nonrigid Motion. *Artificial Intelligence*, 36(1):91–123, 1988.

[20] B.C. Vemuri and A. Radisavljevic. From Global to Local, a Continuum of Shape Models with Fractal. In *Computer Vision and Pattern Recognition*, 307–313, 1993.